# Is It Possible To Correlate a Collection of Copper Nanocrystals with Their Optical Response?

C. Salzemann,[†,‡] J. Lermé,[§] J. Urban,[†] and I. Lisiecki*[,‡]

*Fritz-Haber-Institut der MPG, Abt. AC, 4-6 Faradayweg, D-14195 Berlin, Germany, Laboratoire LM2N, UMR CNRS 7070 Université Pierre et Marie Curie (Paris VI), B.P.52, 4 place Jussieu, F-752 31 Paris Cedex 05, France, and Laboratoire de Spectrométrie Ionique et Moléculaire, CNRS and Université Lyon I, Bâtiment A. Kastler, 43 boulevard du 11 novembre 1918, 69622 Villeurbanne Cedex, France*

*Received June 28, 2004*
*Revised Manuscript Received December 13, 2004*

Nanomaterials are an important research field, especially because changing their size and shape can modify their properties. The control of copper nanocrystal size was obtained, for the first time, in our laboratory in 1993[1,2] and no other similar cases in mixed reverse micelles have been presented since then. However, a very large number of nanomaterials have been produced by using reverse micelles as microreactors.[3] The first generation of copper particles synthesized in reverse micelles is mostly characterized by a spherical shape. Such metallic particles are characterized by diameter varying from 3 to 13 nm. As expected from extended Mie theory,[4−8] an increase in the 560 nm plasmon band and a decrease in its bordering take place on increasing the particle size. In that case, as in many theoretical investigations, the size dependence is phenomenologically introduced by taking into account the so-called surface scattering-limited mean-free-path effect. By changing slightly the synthetic procedure, a small proportion of nonspherical Cu nanocrystals is obtained. In such a case, the optical response shows the appearance of a new resonance around 640 nm. For spherical particles, one collective excitation mode is taken into account. However, with particles having various shapes, several plasmon resonance modes appear to be associated with the various axes of the particles. For instance, ellipsoids having axial symmetry are characterized by 2 resonance modes. These various oscillation modes can be observed when the particles are randomly dispersed. Hence the absorption measurements of particles depend on their shape, the polarization of light, and the various distributions of the particle orientation.[9,10]

In this paper, we focus on the 640 nm resonance band that could be related to a small amount of nonspherical Cu particles. To confirm such a relationship, we present here a theoretical investigation based on the time-dependent local-density-approximation (TDLDA).[11,12]

The synthesis of copper nanocrystals, described in the Appendix, is carried out at two water contents: $w = 1.5$ and $w = 4$. At the end of the synthesis a drop of solution is deposited on a TEM grid.[13] Figure 1A shows the TEM image obtained at $w = 1.5$ with appearance of nanoparticles having an average diameter of 3 nm. The size distribution determined from the histogram in the insert is determined using around 500 particles and is 0.6 nm (18%). In this case, high-resolution transmission electron microscopy, HRTEM, cannot be performed because the particles are embedded in the AOT surfactant. Furthermore, it has to be noted that the observation of such coated particles are all the more difficult that the particle is small. The optical spectrum of the solution,[14] at the end of the synthesis (Figure 2A), shows a continuous smooth absorption with an almost imperceptible shoulder around 560 nm. Synthesis at $w = 4$ shows an increase in the particle size with an average diameter of 8.4 nm (Figure 1B) and a size distribution (insert Figure 1B) of 1.8 nm (20%). The HRTEM images show formation of spherical particles with defects made of fcc clusters (Figure 1C) and of regular decahedra, formed by 5 deformed tetrahedral subunits and characterized by a 5-fold symmetry[15] (Figure 1D). This is confirmed by the calculated power spectra (PS) given in the Figure 1D insert. Note that no other shapes are observed by TEM. The optical spectrum shows a noticeable resonance band around 560 nm and another at 650 nm (Figure 2B). To quantify these changes in the absorption spectra observed in Figure 2, a mixed classical/quantum model is used. The calculations are based on the time-dependent local-density-approximation formalism (DFT-TDLDA) within a model including the absorption and screening properties of both the ionic core background and the surrounding matrix.[12] The ingredients of this model have been detailed and discussed in previous papers[11,12] and are only briefly outlined here. The conduction electrons, responsible for the collective surface plasmon excitation, are quantum-mechanically treated, whereas the ionic background is phenomenologically described by both: (i) a step-walled, homogeneous, spherical charge distribution (jellium) of radius $R$ and (ii) a homogeneous, dielectric medium (core− electron dielectric function $\epsilon_{ib}(\omega)$, corresponding to the interband transitions, assumed to be bulklike) extending up to $R_c = R - d$ where $d$ is the skin thickness of ineffective

* To whom correspondence should be addressed.
† Fritz-Haber-Institut der MPG.
‡ UMR CNRS 7070 Université Pierre et Marie Curie (Paris VI).
§ CNRS and Université Lyon I.

(1) Lisiecki, I.; Pileni, M. P. *J. Am. Chem.* **1993**, *115*, 3887.
(2) Lisiecki, I.; Pileni, M. P. *J. Phys. Chem.* **1995**, *99*, 5077.
(3) Pileni M. P. *Nat. Mater.* **2003**, *2*, 145.
(4) Mie, G. *Ann. Phys.* **1908**, *25*, 377.
(5) Fragstein, C. V.; Roemer, H. *Z. Phys.* **1958**, *151*, 54.
(6) Roemer, H.; Fragstein, C. V. *Z. Phys.* **1961**, *163*, 27.
(7) Fragstein, C. V.; Schoenes, F. J. *Z. Phys.* **1967**, 198, 477.
(8) Fröhlich, H. *Elektronentheorie der Metalle*; Springer; Berlin, 1936.
(9) Kelly, K. L.; Coronado, E.; Zhao, L. L.; Schatz, G. C. *J. Phys. Chem. B* **2003**, *107*, 668.
(10) Sosa, I. O.; Noguez, C.; Barrera, R. G. *J. Phys. Chem. B* **2003**, *107*, 6269.
(11) Lermé, J.; Palpant, B.; Prével, B.; Pellarin, M.; Treilleux, M.; Vialle, J. L.; Perez, A.; Broyer, M. *Phys. Rev. Lett.* **1998**, *80*, 5105.
(12) Lermé, J. *Eur. Phys. J. D* **2000**, *10*, 265.
(13) Transmission electron micrographs (TEM) were obtained using a Philips CM200 FEG microscope operating at 200 kV, Cs = 1.35 mm with an information limit better than 0.18 nm. Both overview images and high-resolution images were performed.
(14) Absorption spectra were recorded on a conventional Varian Cary 1 spectrophotometer.
(15) Urban, J. *Cryst. Res. Technol.* **1998**, *33* (7), 1009.

10.1021/cm048970z CCC: $30.25 
Published on Web 02/18/2005

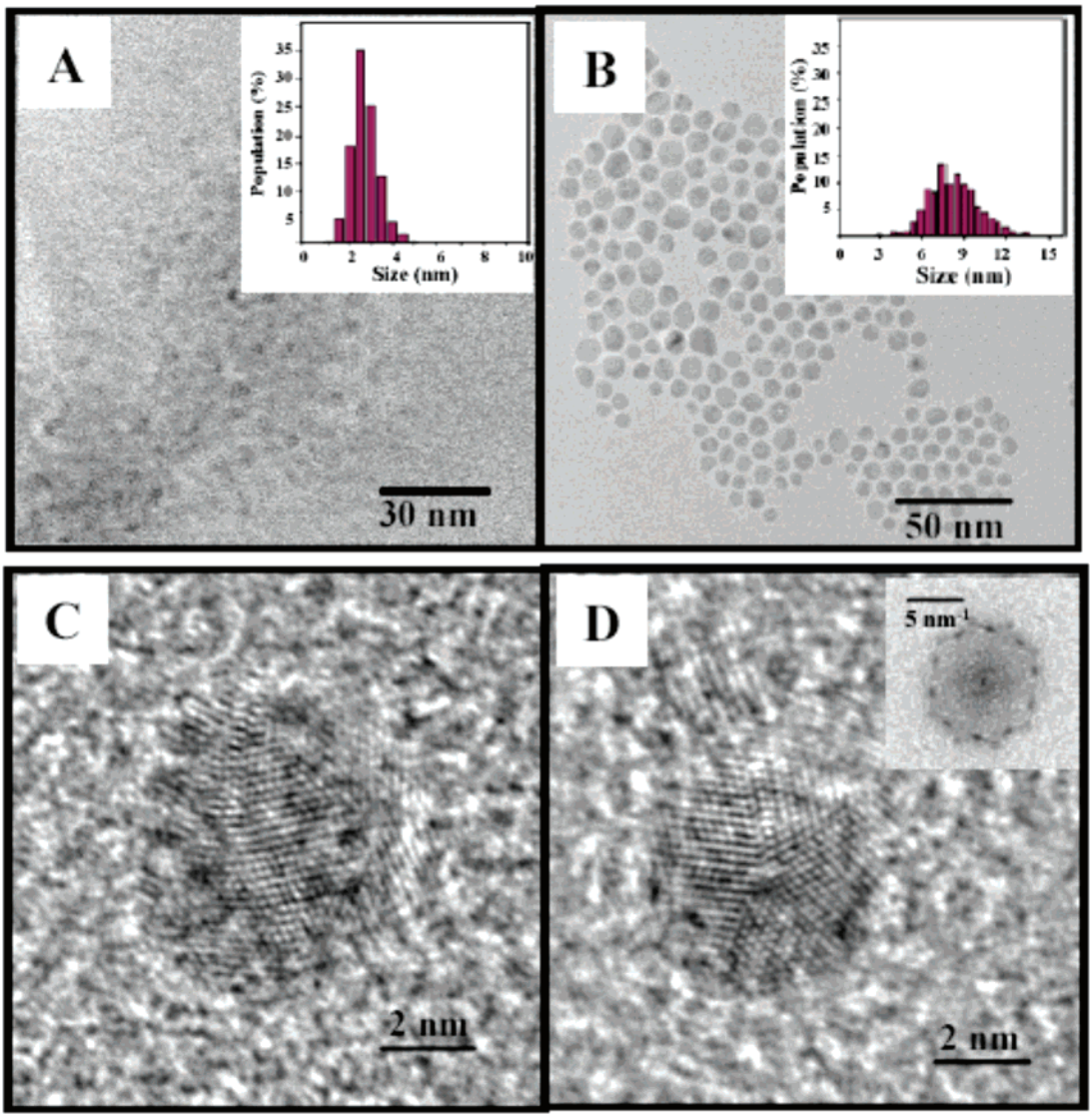


**Figure 1.** Electron microscopy patterns of copper metallic particles synthesized in $Cu(AOT)_2$/NaAOT, water, isooctane reverse micelles at various water contents. [AOT] = 0.1 M; $[Cu(AOT)_2] = 10^{-2}$ M. [A] $w = 1.5$; [B] $w = 4$. Inserts: Size histograms [C] and [D] HRTEM images of copper nanocrystals synthesized at $w = 4$. Insert of Figure 1D: power spectrum of the HRTEM image.

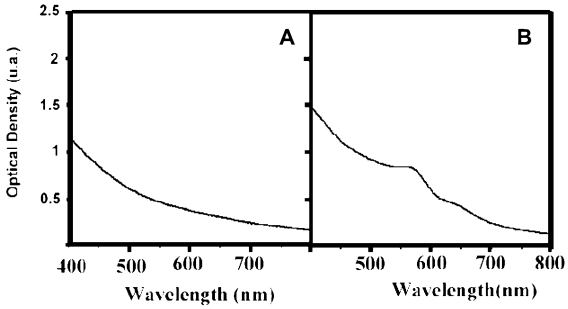


**Figure 2.** Absorption spectra of copper metallic particles synthesized in $Cu(AOT)_2$/NaAOT, water, isooctane reverse micelles at various water contents. [AOT] = 0.1 M; $[Cu(AOT)_2] = 10^{-2}$ M. [A] $w = 1.5$; [B] $w = 4$.

ion polarizability. This ingredient, introduced early by Liebsh[16] and discussed later by several authors,[11,17,18] is partly related to the spatial localization of the d-electron wave functions (the value $d = 3$ au has been selected in the present work). The core−electron dielectric function $\epsilon_{ib}(\omega)$ has been carefully extracted from the experimental dielectric function $\epsilon_{exp}(\omega)$ of bulk copper[19] by a Kramers−Kronig (KK) analysis.[20] For this determination we assumed the following parameters entering the free-electron Drude contribution $\epsilon_s(\omega)$ to the overall dielectric function $\epsilon_{exp}(\omega) = \epsilon_s(\omega) + \epsilon_{ib}(\omega) - 1$: effective electron mass $m/m_e = 1.42$[20] ($m_e$ is the free electron mass), Wigner-Seitz radius $r_s = 2.67$ bohr[21] and scattering rate $\Gamma(\infty) = 0.12$ eV (deduced from the KK analysis in the spectral range around the interband threshold). For the surrounding matrix, we assumed the dielectric constant $\epsilon_m = 2$, appropriate to the visible spectral range. Let us remark however that this value could be questioned because of the presence of surfactant molecules on the particle surface and in view of the sensitivity of the plasmon frequency to the metal/matrix interface. For instance, in the

(16) Liebsch, A. *Phys. Rev.* **1993**, *48*, 11317.
(17) Kresin, V. V. *Phys. Rev. B* **1995**, *51*, 1844.
(18) Serra, Ll.; Rubio, A. *Z. Phys.* D **1997**, *40*, 262.
(19) Palik, E. D. *Handbook of optical constants of solids*; Academic: New York, 1985; Vol. I. Palik, E. D. *Handbook of optical constants of solids*; Academic: New York, 1991; Vol. II.
(20) Ehrenreich, H.; Philipp, H. R. *Phys. Rev.* **1962**, *128*, 1622.
(21) Kittel, C. *Introduction to solid-state physics*; John Wiley and Sons Inc.: New York, 1983.

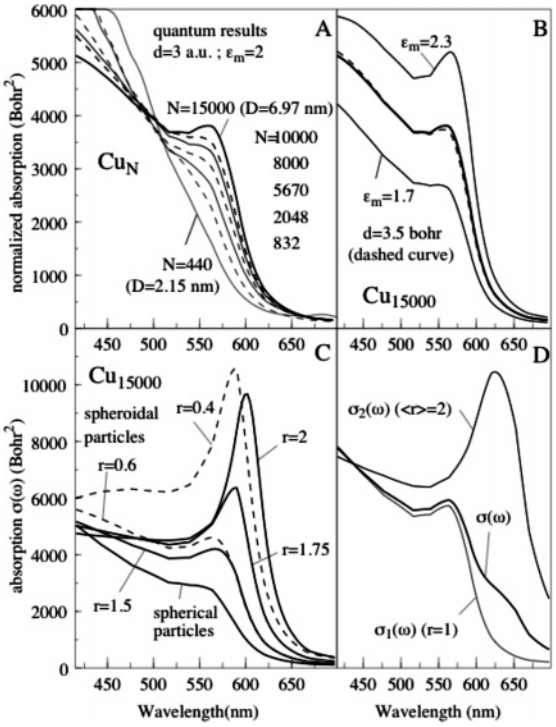


**Figure 3.** [A] Absorption cross sections calculated with the classical/quantal model (TDLDA formalism), for various particle sizes containing $N = 440$, 832, 2048, 5670, 8000, 10000, 15000 atoms. To plot the absorption spectra in the same figure, the theoretical data (in bohr$^2$) have been multiplied by the volume ratio 15000/$N$ (the $y$-axis corresponds thus only to the largest size $N = 15000$). [B] Sensitivity of the absorption cross section to the input parameters, for the size $N = 15000$ ($\epsilon_m$ is the dielectric constant of the solvent and $d$ is the thickness of the surface skin of ineffective ionic core polarizability). The thick-line absorption curve corresponds to the values $\epsilon_m = 2$ and $d = 3$ bohr. The dashed line curve corresponds to the values $\epsilon_m = 2$ and $d = 3.5$ bohr. The upper and lower thin-line curves correspond to the values $\epsilon_m = 2.3$ and $\epsilon_m = 1.7$, respectively ($d = 3$ bohr). [C] Absorption cross sections for spheroidal distortions of the particles (classical calculations involving coated particles). $r$ is the ratio of the major principal axis of the particle (axis of revolution) to the minor principal axis: $r = 1 \rightarrow$ sphere; $r > 1 \rightarrow$ cigar-shaped spheroids; $r < 1 \rightarrow$ pancake-shaped spheroids (dashed line curves). [D] Simulation of the experimental absorption spectrum corresponding to the sample $w = 4$. This simulation takes into account the size distribution of the clusters in the sample. The colloidal dispersion is assumed to consist of two distinct $Cu_N$-cluster populations. The first involves spherical particles (axis ratio $r = 1$); the second involves cigar-shaped spheroids with axis-ratios $r$ distributed around the mean value $\langle r \rangle = 2$. The lower thin line curve [$\sigma_1(\omega)$] and the dashed line curve [$\sigma_2(\omega)$] are absorption spectra that are obtained if all the particles belong either to the first or to the second population, respectively. Assuming that the two populations contain 80% and 20% of the clusters, respectively, one obtains the absorption spectrum $\sigma(\omega) = 0.8\sigma_1(\omega) + 0.2\sigma_2(\omega)$ [thick line curve].

case of a solid matrix like amorphous alumina the influence of the local porosity at the interface was clearly pointed out.[11] Thus, additional calculations have been carried out in order to estimate the impact of the selected $\epsilon_m$ value, as well as those of other physical parameters.

The absorption cross sections calculated for various particle sizes are shown in Figure 3A. Since the magnitude of the cross section scales roughly as the particle volume, the theoretical data have been multiplied by the factor 15000/$N$ (the $y$-axis corresponds thus to the largest size). This allows plotting of all the spectra in the same figure and makes the size evolution of the resonance band more apparent. The resonance band (around $\lambda \approx 560$ nm) emerges gradually from the rising edge of the interband transitions (the interband threshold is 1.9 eV). Similar behavior is observed for gold clusters (for gold the resonance band is however much more apparent[22]). The damping and broadening of the resonance band is actually a direct signature of a slight blue-shift—inside the interband-transition spectral range—of the resonance frequency as the size decreases. The sensitivity of the absorption cross section to the input parameters does not depend noticeably on the thickness of the surface skin of ineffective polarizability [the value $d = 3.5$ au (determined by comparison with experimental data on free $Ag_N^+$ clusters) is used for gold and silver;[11] the value $d = 3$ au is assumed for copper in view of the lower $r_s$ value of this element and consequently the smaller ion-core size]. On the other hand, the emergence of the resonance band depends noticeably on the refractive index of the surrounding matrix (Figure 3B). Obviously, this is due to the fact that the emergence (in other terms the damping) of the surface plasmon resonance is strongly dependent on the location of the plasmon frequency relative to the interband threshold. As observed in the experiment (Figure 2) and simulation (Figure 3A), the resonance band (around $\lambda \approx 560$ nm) emerges from the rising edge of the interband transitions. Hence, from simulation and experiments, the resonance at 560 nm is attributed to the surface plasmon excitation of spherical nanocrystals. These data are consistent with what is observed by TEM and HRTEM images in Figure 1. However, Figure 2B shows another absorption peak around 650 nm that is not expected from the TEM images shown in Figure 1B. The first idea is that the shoulder could be due to an artifact. So to make sure, the experiments were reproduced several times using various spectrophotometers. Furthermore, when the spectra are characterized by both the 560 nm peak and the shoulder at around 640 nm, the kinetic study always shows that the latter one emerges before the first one.[23] This indicates that the absorption at 640 nm could be mainly due to seeds that are still present at the end of the synthesis. However, it has been impossible to observe them. These seeds could have various shapes such as decahedral, cuboctahedral, and tetrahedral.[23,24] Since quantum calculations are too time-consuming for spheroidal particle shapes, a classical description (exact formulas are available for ellipsoids) is used for the present purpose. Since the influence of the surface skin of ineffective polarization is essential for interpreting the optical properties of noble metal clusters, calculations involving coated ellipsoids (two nested ellipsoids having the same focuses) have been carried out.[25,26] We denote by $a$ and $a'$ the semi-axes of revolution (major axes) of the inner and outer ellipsoids, respectively, and by $b$ and $b'$ the minor (2-fold degeneracy) semi-axes. The axis-ratio $r$

(22) Palpant, B.; Prével, B.; Lermé, J.; Cottancin, E.; Pellarin, M.; Treilleux, M.; Perez, A.; Vialle, J. L.; Broyer, M. *Phys. Rev B* **1998**, *57*, 1963.
(23) Salzemann C.; Lisiecki I.; Brioude A.; Urban J.; Pileni M. P. *J. Phys. Chem. B* **2004**, *108*, 13242.
(24) Kirkland, A. I.; Jefferson, D. A.; Duff, D. G.; Edwards, P. P.; Gameson, I.; Johnson, B. F. G.; Smith, D. J. *Proc. R. Soc. London A* **1993,** *440*, 589.
(25) Bohren, C. F.; Huffman, D. R. *Absorption and scattering of light by small particles*; John Wiley and Sons: New York, 1998.
(26) Berthier, S. *Optique des milieux composites*; polytechnica: Paris, 1993.
(27) Copper bis(2-ethylhexyl) sulfosuccinate, $Cu(AOT)_2$, has been prepared as described previously.[28]
(28) Petit, C.; Lixon, P.; Pileni, M. P. *Langmuir* **1991**, *7*, 2620.
(29) Sodium bis(2-ethylhexyl) sulfosuccinate, Na(AOT), has been purchased from Fluka.

$= a'/b'$ characterizes the overall shape of the particle: $r = 1$ (sphere), $r > 1$ for cigar-shaped (prolate) ellipsoids and $r < 1$ for pancake-shaped (oblate) ellipsoids. The axes of both ellipsoids (same focuses) are related by $a'^2 = a^2 + u$ and $b'^2 = b^2 + u$. Since the skin thickness is small relative to the particle size, we have approximately $(a' - a) \approx u/2a$ and $(b' - b) \approx u/2b$, indicating that the skin thickness is larger along the smaller axis. To partly compensate for the fact that the quantum spillout effect[11,12] (leading to a red-shift of the resonance frequency, opposite to the shift induced by the skin of ineffective ion polarizability) is not taken into account in the classical model, the parameter $u$ has been chosen, for each size, in such a way that $(b' - b) = d = 3$ au. The surface-averaged skin thickness is therefore lower than $d = 3$ au; furthermore, $r$ differs from unity. The dielectric functions, inside the inner ellipsoid, in the skin region, and beyond the outer ellipsoid are $\epsilon_3 = \epsilon_s(\omega) + \epsilon_{ib}(\omega) - 1$, $\epsilon_2 = \epsilon_s(\omega)$, and $\epsilon_1 = \epsilon_m$, respectively. Assuming that the ellipsoidal particles are randomly oriented, the absorption cross section, in the dipolar approximation (quasi-static), is given by (atomic units)

$$\sigma(\omega) = \frac{4\pi\omega}{c\epsilon_m^{1/2}} \frac{1}{3}\sum_{i=1}^{3}\{Im\}[\alpha_i(\omega)] \tag{1}$$

$$\alpha_i(\omega) = \frac{a'b'^2}{3}\epsilon_1 \times \frac{(\epsilon_2 - \epsilon_1)[\epsilon_2 + (\epsilon_3 - \epsilon_2)(A_i - pA_i')] + p\epsilon_2(\epsilon_3 - \epsilon_2)}{[\epsilon_2 + (\epsilon_3 - \epsilon_2)(A_i - pA_i')][\epsilon_1 + (\epsilon_2 - \epsilon_1)A_i'] + pA_i'\epsilon_2(\epsilon_3 - \epsilon_2)} \tag{2}$$

The $\alpha_i(\omega)$'s are the dynamical polarizabilities of the particle along the three principal axes, $p = ab^2/a'b'^2$ is the fraction of the total particle volume occupied by the inner ellipsoid, and the $A_i$ and $A_i'$ are the geometrical depolarization factors of the inner and outer ellipsoids along the three principal axes (these factors are functions of the eccentricities of the ellipsoids). The standard Mie's formula for the sphere ($A_i' = 1/3$) is recovered when $\epsilon_3$ and $\epsilon_2$ are identical. Ellipsoids having axial symmetry (spheroids) are considered. Some results obtained for the cluster size containing $N = 15000$ atoms (volume $= 4\pi a'b'^2/3 = 4\pi r_s^3 N/3$) are presented in Figure 3C. These calculations point out the strong dependence of the absorption cross section on the shape of the particle. For simple metal particles [$\epsilon(\omega) \approx \epsilon_s(\omega)$; $\epsilon_{ib}(\omega) \approx 1$] ellipsoidal distortions lead to the removal of the 3-fold degeneracy of the dipolar surface plasmon resonance, and two (spheroids) or three (triaxial ellipsoids) resonance bands are clearly observed. In the case of noble metal clusters, only the low-energy resonances, which correspond to the oscillation of the conduction electron gas along the largest principal axis, are observed because the high-energy ones are completely damped by the interband transitions. Let us remark that, in the classical absorption spectrum corresponding to the sphere ($N = 15000$; $d = 3$ au), the resonance band is reflected through a shoulder on the rising edge of the interband transitions. From Figures 3A and 3C one can see that the deformed particles, even though present in very small proportion, contribute largely in the low-energy spectral range; furthermore, the axis-ratio $r$ differs from unity. From the analysis of the absorption spectra shown in Figure 2B, it is assumed that the colloidal solutions used for the absorption experiments consist of two distinct $Cu_N$-particle populations (labeled by the indexes 1 and 2, respectively): the first involves spherical particles ($r = 1$, size distribution only); the second involves ellipsoidal prolate clusters (size and shape distributions). The shape distribution is parametrized by a normalized Gaussian $r$-function $g(r) \propto \exp[-(r - \langle r\rangle)^2/2(\Delta r)^2]$ characterized by its maximum $\langle r\rangle$ and the standard deviation $\Delta r$. The experimental absorption spectrum is quite well reproduced in assuming there is spherical symmetry for most of the particles (80%) and a shape distribution for the second population (20% of the particles) characterized by $\langle r\rangle = 2$ and $\Delta r = 0.5$, namely, $\sigma(\omega) = 0.8\sigma_1(\omega) + 0.2\sigma_2(\omega)$. Figure 3D represents the absorption spectra corresponding to both populations [$\sigma_1(\omega)$ and $\sigma_2(\omega)$]. There is rather good agreement between experiment (Figure 2B) and simulation (Figure 3D) for the synthesis made at $w = 4$ with appearance of a shoulder around 640 nm is found. From these data, it seems that a slight deformation of particle shape largely contributes to the low-energy spectral range. Note that, in the transmission electron micrograph corresponding to the sample $w = 4$ (Figure 2B), most of the particles exhibit facets. Therefore, it is concluded that the main influence of the observed deformations will consist in a slight smoothing of the resonance band centered around 560 nm. The resonance band for the sphere in Figure 3C ($N = 15000$; $D \approx 7$ nm) is much more damped than in Figure 3D, although the simulation of the experimental spectrum involves a broad size distribution. As a matter of fact, since the absorption scales as the particle volume, the spectrum in Figure 3D reflects mainly the absorption from the largest particles. For very large clusters, the blue-shift of the plasmon frequency induced by the surface skin of ineffective polarizability is quite negligible and the absorption cross section no longer depends on the size, except for a mere scaling volume factor. For $r = 2$ the low-energy resonance in Figure 3D [$\sigma_2(\omega)$] is centered around $\lambda \approx 625$ nm, whereas it is centered around $\lambda \approx 600$ nm in Figure 3C. The fact that a slight deformation induces a large change in the spectrum in the low-energy range [axis-ratios $r > 2$ are involved in Figure 3D] and the absorption reflecting the largest particles could explain this apparent inconsistency.

Nevertheless, the presence of nuclei having various shapes such as decahedral, cuboctahedral, and tetrahedral and/or other anistropic shape nanocrystals cannot be excluded. To confirm this hypothesis, new simulations such as the discrete dipole approximation (DDA)[23] have to be performed. The DDA method is a numerical method in which the object studied is represented as a cubic lattice of $N$ polarizable point dipoles. By this way, the geometry of the particles, whatever their shape, is rigorously taken into account in the calculations (the TDLDA formalism would be much too time-consuming, and very likely technically impracticable, for dealing with such large particles having anisotropic shapes). On the other hand, due to van der Waals interactions between nanocrystals, the presence in solution of a small proportion of groups of two or three (or more) close clusters forming

very small chains could also provide a good explanation.[30,31] Moreover, it must be noted that optical spectra are related to the population of all the nanocrystals present in solution; in this way, it is probably more representative than that of the observed TEM images.

In this paper, we have shown that mainly spherical copper nanocrystals are produced in mixed reverse micelles. However, the corresponding absorption spectra show two resonance bands. One is located around 560 nm and corresponds to the 3-fold degenerate surface plasmon resonance of spherical copper particles. The size dependence of the broadening and damping of this band is in good agreement with simulations. The second resonance band, located around 640 nm, could be the optical signature attributed to cigar-shaped spheroids, or short linear chains characterized by an effective aspect ratio close to 2. Nevertheless, the presence of seeds with various shapes such as decahedral, cuboctahedral, and tetrahedral and/or other anistropic shape nanocrystals cannot be excluded.

**Appendix: Synthesis of Copper Nanocrystals.** Colloidal copper nanocrystals are obtained by mixing two solutions. The first is a mixed micellar solution of copper[27] and sodium bis(2-ethylhexyl) sulfosuccinate[29] usually called AOT. The surfactant concentrations are kept constant ([AOT] = 0.1 M; $[Cu(AOT)_2] = 10^{-2}$ M) in isooctane. The second contains the hydrazine used as the reducing agent. The ratio of the hydrazine concentration to the $Cu(AOT)_2$ concentration is 3. The overall water content, defined as $w = [H_2O]/[AOT]$, varies from 1.5 to 4. The reaction takes place for 3 h. A few drops of solution are deposited on a copper grid covered by amorphous carbon; then, after total evaporation of the solvent, nanocrystals are observed by TEM. To avoid metal oxidation, all of the synthesis is carried out in a glovebox with a nitrogen flow.

CM048970Z

(30) Clippe, P.; Evrard, R.; Lucas, A. A. *Phys. Rev. B* **1976**, *14*, 1715.
(31) Granqvist, C. G.; Hunderi, O. *Phys. Rev. B* **1977**, *16*, 3513.